Journal of Molecular Structure 1277 (2023) 134851

Contents lists available at ScienceDirect

Journal of Molecular Structure

journal homepage: www.elsevier.com/locate/molstr

Two organic-inorganic manganese(II) halide hybrids containing protonated N,N'-dialkylthioureas with efficient green-emission

Nicolay N. Golovnev[a], Marina A. Gerasimova[a], Ivan A. Ostapenko[a], Andrey O. Zolotov[a], Maxim S. Molokeev[a,b,c,*]

[a] Siberian Federal University, Krasnoyarsk 660041, Russia
[b] Laboratory of Crystal Physics, Kirensky Institute of Physics, Federal Research Center KSC SB RAS, Krasnoyarsk 660036, Russia
[c] Research and Development Department, Kemerovo State University, Kemerovo, 650000, Russia

ARTICLE INFO

Article history:
Received 22 October 2022
Revised 18 December 2022
Accepted 21 December 2022
Available online 23 December 2022

Keywords:
Zero-dimensional hybrid manganese(II) halides
N,N′-alkylthioureas
Synthesis
Structure
Photoluminescence
Quantum yield
X-ray diffraction

ABSTRACT

Luminescent $(C_5H_{13}N_2S)_2[MnBr_4]$ (**1**) and $(C_7H_{17}N_2S)_2[MnBr_4]$ (**2**) ($C_5H_{12}N_2S$ = N,N′-diethylthiourea, $C_7H_{16}N_2S$ = N,N′-diisopropylthiourea) were prepared via solvothermal method, and the structures of these compounds have been resolved using X-ray single crystal diffraction. The structures consist of electrostatically bound $MnBr_4^{2-}$ anions and organic $C_5H_{13}N_2S^+$ and $C_7H_{17}N_2S^+$ cations. The intermolecular N−H···Br and N−H···S hydrogen bonds additionally stabilize crystal structures of **1**-**2**. Upon excitation over broadband covering the range 265 to 515 nm, these compounds show green emission peaking at 526 nm for **1** and 522 nm for **2**, which is assigned to the $^4T_1 \rightarrow {}^6A_1$ electronic transition of Mn^{2+} from isolated within the crystal structures $MnBr_4^{2-}$ tetrahedra. The photoluminescence quantum yield (PLQY) of powder **1** is 97 ± 7% for excitation at 440 nm and that of powder **2** is 83 ± 7% for excitation at 365 nm. The high PLQY indicates the absence of noticeable concentration quenching at shortest Mn···Mn distance of 8.11 and 8.73 Å between Mn^{2+} ions within the structures of **1** and **2**. The high-performance photoluminescence of 0D $(C_5H_{13}N_2S)_2[MnBr_4]$ and $(C_7H_{17}N_2S)_2[MnBr_4]$ compounds demonstrated promising applications in photonics.

1. Introduction

Mn-based hybrid organic-inorganic halides have been widely expanded due to their unique advantages, such as solution-process, low cost, environmental friendliness, stability and large-scale production [1–18]. They show superior bright and size-tunable photoluminescence [3,15]. Mn-based hybrid halides can be considered as a very good alternative of toxic lead compounds [19–21]. It has been summarized that Mn^{2+} ions in an octahedral environment usually give out red emissions, while those with tetrahedrally coordinated Mn^{2+} ions tend to emit green emissions [2,5,11,13]. Zero-dimensional (0D) organo-inorganic hybrid manganese(II) halides containing isolated anions MnX_4^{2-} (X = Br, Cl) exhibit green emission with a large Stokes shift and a high photoluminescence quantum yield (PLQY) that can reach 100% [6,22]. It is assumed that the emission of the tetrahedral coordinated Mn(II) ions originates from the *d*–*d* ($^4T_1 \rightarrow {}^6A_1$) transition [2–8]. Protonated primary, secondary, and tertiary amines, as well as quaternary ammonium and phosphonium bases cations (for instance, [23–27]) as organic components of hybrid metal halides (HMHs) are commonly used. Much less studied are compounds containing S-protonated organic substances, for example, thiourea and its N-substituted derivatives, the ability of which to form singly charged S-protonated cations in strongly acidic solutions is well known [28]. Among HMHs, only a few compounds containing protonated thiourea ($CH_5N_2S^+$) have been structurally characterized, for example $(CH_5N_2S)_2(CH_5N_2)_2[PbI_4]$ [29], $(CH_5N_2S)_3(CH_6N)_2[Pb_2I_9]$ and $(CH_5N_2S)_3[PbI_5]$ [30], $(CH_5N_2S)(CH_6N)_2[Pb_2I_7]$ [31], $(CH_5N_2S)_2[OsX_6]$ (X = Cl, Br) [32], and $(CH_5N_2S)_6[BiBr_6]Br_3$ [33]. There are no such data for N-substituted thioureas, although their HMH compounds may have unique photo-physical properties and find practical applications. In this work, two N,N′-dialkylthioureas are introduced into hybrid halide materials. We reported the synthesis and properties of the novel 0D organic–inorganic hybrid crystals $(C_5H_{13}N_2S)_2[MnBr_4]$ and $(C_7H_{17}N_2S)_2[MnBr_4]$ ($C_5H_{13}N_2S$ = monoprotonated N,N′-diethylthiourea, $C_7H_{17}N_2S$ = monoprotonated N,N′-diisopropylthiourea), which exhibit highly efficient green-light emission with a high PLQY.

* Corresponding author at: Maxim Molokeev, Laboratory of Crystal Physics, Kirensky Institute of Physics, Federal Research Center KSC SB RAS, bld. 38 Akademgorodok 50, Krasnoyarsk 660036, Russia
E-mail address: msmolokeev@gmail.com (M.S. Molokeev).

https://doi.org/10.1016/j.molstruc.2022.134851
0022-2860/

Table 1
The crystal structure parameters of $(C_5H_{13}N_2S)_2[MnBr_4]$ and $(C_7H_{17}N_2S)_2[MnBr_4]$.

Chemical formula	$C_{10}H_{26}Br_4MnN_4S_2$	$C_{14}H_{34}Br_4MnN_4S_2$
Molecular weight	641.04	697.15
Temperature (K)	293	296(2)
Space group, *Z*	*P*-1, 2	*C*2/*c*, 4
a (Å)	8.1221(12)	20.982(2)
b (Å)	11.8965(17)	9.6482(10)
c (Å)	12.1442(18)	15.7844(16)
α (°)	90.541(3)	90
β (°)	93.921(3)	119.414(2)
γ (°)	94.893(4)	90
V (Å^3)	1166.3(3)	2783.5(5)
ρ_{calc} (g/cm^3)	1.820	1.664
μ (mm^{-1})	7.596	6.372
Reflections measured	9656	14301
Reflections independent	3614	2839
Reflections with $F > 4\sigma(F)$	2464	1757
$2\theta_{max}$ (°)	47.78	52.734
h, k, l - limits	-9 ≤ *h* ≤ 9; -13 ≤ *k* ≤ 13; -13 ≤ *l* ≤ 13	-26 ≤ *h* ≤ 26; -12 ≤ *k* ≤ 12; -19 ≤ *l* ≤ 19
R_{int}	0.0537	0.0915
Refinement results		
The weighed refinement of F^2	$w=1/[\sigma^2(F_o^2)+(0.0447P)^2+0.8800P]$ where $P=\max(F_o^2+2F_c^2)/3$	$w=1/[\sigma^2(F_o^2)+(0.0716P)^2+6.5540P]$ where $P=\max(F_o^2+2F_c^2)/3$
Number of refinement parameters	205	118
*R*1 [$F_o > 4\sigma(F_o)$]	0.0435	0.0616
*wR*2	0.0969	0.1415
Goof	1.020	1.038
$\Delta\rho_{max}$ (e/Å^3)	0.751	0.527
$\Delta\rho_{min}$ (e/Å^3)	-0.496	-0.416
$(\Delta/\sigma)_{max}$	<0.001	<0.001
Extinction coefficient (SHELXL 2014/7)	0.0105(8)	0.0022(3)

2. Experimental section

2.1. Reagents

The reagents N,N'-diethylthiourea and N,N'-diisopropylthiourea were obtained from Sigma–Aldrich. $MnBr_2$, $Mn(CH_3COO)_2{\cdot}4H_2O$ and HBr were of analytical grade. All reagents were used without any additional purification.

2.2. Synthesis of crystals 1 and 2

The 0.20 g of N, N'-diethylthiourea (DETU) was dissolved in 1 mL HBr, then crystalline manganese(II) acetate was added. Molar ratio DETU:$Mn(CH_3COO)_2{\cdot}4H_2O$ was equal to 2:1. On standing in air of two-phase liquid system for 2-3 weeks, large needle-like crystals of bright yellow-green color were formed. These crystals were filtered off and dried between sheets of filter paper at room temperature. Yield of compound **1** is 72% (0.36 g). When using $MnBr_2$, precipitation often occurred after a month or more. Upon addition of a small crystal of the previously obtained compound, powder precipitation occurred instantaneously with both manganese acetate and manganese bromide. This behavior may be associated with the formation of stable the $(C_5H_{12}N_2S)_2[MnBr_4]$ supersaturated aqueous solutions.

More easily was obtained $(C_7H_{17}N_2S)_2[MnBr_4]$. In a typical experiment, 0.5 mL of HBr is added to a mixture of 0.30 g (1.40 mmol) $MnBr_2$ and 0.45 g (2.80 mmol) N,N'-isopropylthiourea. The resulting two-phase liquid system at 80°C turns into a single-phase solution (but upon cooling, phase separation occurred again). The solution was kept at 80°C to a volume of 0.5 mL and then slowly was cooled to room temperature. For 1-2 days a pale green precipitate formed which was filtered off and dried between sheets of filter paper in air at room temperature. Yield of compound **2** is 58% (0.57 g).

The single crystals of **1** and **2** for the X-ray diffraction analysis were directly selected from the total mass of the corresponding precipitates. All attempts to synthesize analogous N,N'-dimethylthiourea and N,N'-dibutylthiourea compounds failed.

2.3. X-ray diffraction analysis

The intensity patterns were collected from single crystal $(C_5H_{13}N_2S)_2[MnBr_4]$ and $(C_7H_{17}N_2S)_2MnBr_4$ at 296 K using the SMART APEX II single crystal diffractometer (Bruker AXS, analytical equipment of Krasnoyarsk Center of collective use of SB RAS) equipped with a CCD-detector, graphite monochromator and Mo K_α radiation source. Space groups *P*-1 for **1** and *C*2/*c* for **2** were determined from the statistical analysis of the intensities of all the reflections. The absorption corrections were applied using the SADABS program. The structures were solved by the direct methods using package SHELXS and refined in the anisotropic approach for all atoms using the SHELXL program [34]. Almost all hydrogen atoms of the $C_5H_{13}N_2S^+$ and $C_7H_{17}N_2S^+$ ions were positioned geometrically as riding on their parent atoms with *d*(C–H) = 0.97 Å for the C–H bonds and $U_{iso}(H) = 1.2U_{eq}(C)$. The hydrogen atom near S, N atoms were localized using electron difference pattern and refined with restrictions on bond length. Two atoms N2B and C4B in one molecule of $(C_5H_{13}N_2S)_2[MnBr_4]$ were disordered over two sites due to large thermal parameters. The hydrogen atoms of corresponding disordered motif were not presented and refined, however chemical formula accounts these atoms. Four atoms N2, C6, C7, C8 in $(C_7H_{17}N_2S)_2MnBr_4$ crystal were also refined over two sites, and corresponding H atoms were also omitted. The structure test for the presence of missing symmetry elements and possible voids was produced using the program PLATON [35]. The main crystal data are shown in Table 1. The crystallographic data are deposited in Cambridge Crystallographic Data Centre (CCDC # 2208046-2208047). The data can be down loaded from the site (www.ccdc.cam.ac.uk/data_request/cif). The coordi-

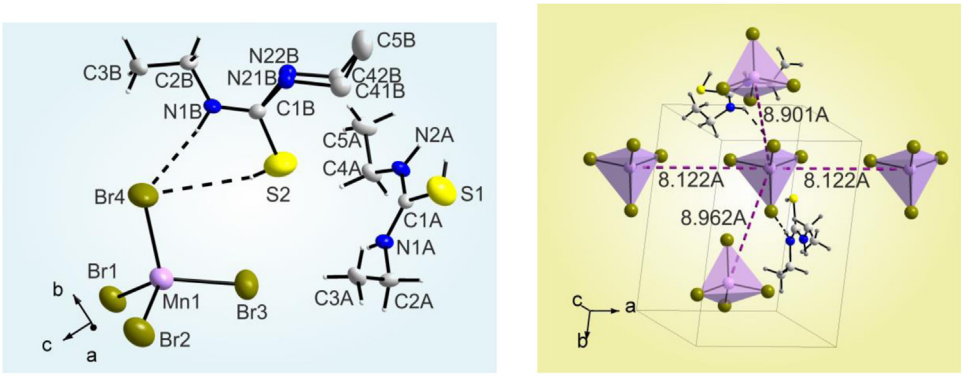

a) b)

Fig. 1. Crystal structure of $(C_5H_{13}N_2S)_2[MnBr_4]$ in the asymmetric part of the unit cell (a). The hydrogen bonds are presented by dashed lines. The thermal ellipsoids are drawn at the 50% probability level. (b) The Mn···Mn contacts and closest coordination of $MnBr_4$.

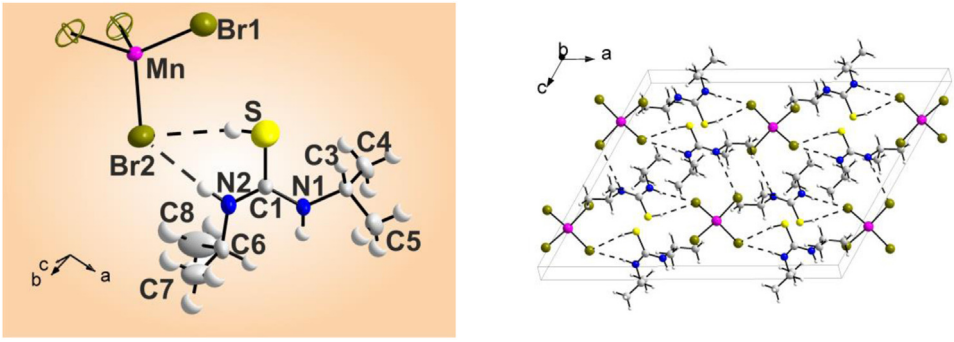

a) b)

Fig. 2. Crystal structure of $(C_7H_{17}N_2S)_2[MnBr_4]$ (a). The atoms in the asymmetric part (b) of the unit cell are labeled, the hydrogen bonds are presented by dashed lines. The thermal ellipsoids are drawn at the 50% probability level.

nates of atoms are given in Table S1. The main bond lengths and angles of **1** and **2** are shown in Table S2, S3. The DIAMOND program [36] was used for the crystal structure plotting (Figs. 1, 2).

Powder X-ray diffraction data of $(C_5H_{13}N_2S)_2[MnBr_4]$ and $(C_7H_{17}N_2S)_2[MnBr_4]$ were obtained using diffractometer D8 ADVANCE (Bruker, analytical equipment of Krasnoyarsk Center of collective use of SB RAS) equipped by a VANTEC detector with a Ni filter. The measurements were made using Cu Kα radiation. The structural parameters defined by single crystal analysis were used as a basic in powder pattern Rietveld refinement. The refinement was produced using program TOPAS 4.2 [37]. Low *R*-factors (Table S4, S5) and good refinement results shown in (Figs. S1, S2) indicate the crystal structures of the powder samples to be representative one of the bulk structures.

2.4. Measurements of thermal stability

Thermogravimetric (TG) and differential scanning calorimetry (DSC) analysis of synthesized compounds **1** and **2** was carried out on a NETZSCH STA 409 PC/PG Thermal Analyzer under the dynamic argon atmosphere (15 mL/min flow rate) within 25–500°C at the scan rate of 10°C/min. The sample weight was 5.570 mg for **1** and 6.730 mg for **2**. Platinum crucibles with perforated lids were used as containers.

2.5. Measurements of photoluminescent properties

The photoluminescence (PL) and photoluminescence excitation (PLE) spectra of powders **1-2** were recorded on a Horiba Scientific Fluorolog 3–22 spectrofluorometer. The absorption spectra were measured on a PerkinElmer Lambda 35 spectrophotometer with an integrating sphere. The emission of powders were carried out at different excitation wavelengths of 275-500 nm. The PL spectra were corrected to the following distorting factors: spectral sensitivity of PMT, different intensity of excitation, and the background. All spectral measurements were performed at a room temperature using the front face geometry. Under experimental conditions, the samples were stable to the UV irradiation. The photoluminescence quantum yield was measured using the integrating sphere RTC-060-SF (Newport, USA), spectrometer with fiber-optic input Maya2000 (Ocean Optics, USA) and four LEDs: L365A, L385A, L405A, L475 (Ocean Optics, USA) and one standard LED peaking 440 nm.

3. Results and discussion

3.1. Crystal structures of 1 and 2

The structure $(C_5H_{13}N_2S)_2[MnBr_4]$ determined by single crystal X-ray diffraction (SCXRD) adopts a triclinic space group *P*-1. The asymmetric part of the $(C_5H_{12}N_2S)_2MnBr_4$ unit cell contains two ions of $C_5H_{12}N_2S^+$, one Mn^{2+} and four Br^- ions (Fig. 1a). The Mn^{2+} ion is connected with four Br^- ions and forms $MnBr_4^{2-}$ tetrahedron. The distorted tetrahedra are isolated with each other with Mn–Br bond lengths between 2.4819(14) and 2.5200(12) Å (Table S2). The Br–Mn–Br angles are varied from 107.05(5) to 111.75(5)°. These values of bond lengths and bond angles are close to those found in the reported $MnBr_4$ tetrahedrons [4–27]. The tetrahedrons are isolated from each other by bulky $C_5H_{13}N_2S^+$ ions. The closest Mn···Mn distance within the crystal is 8.1114(13) Å (Fig. 1b). There are two N–H···Br and two S–H···Br hydrogen bonds (Table

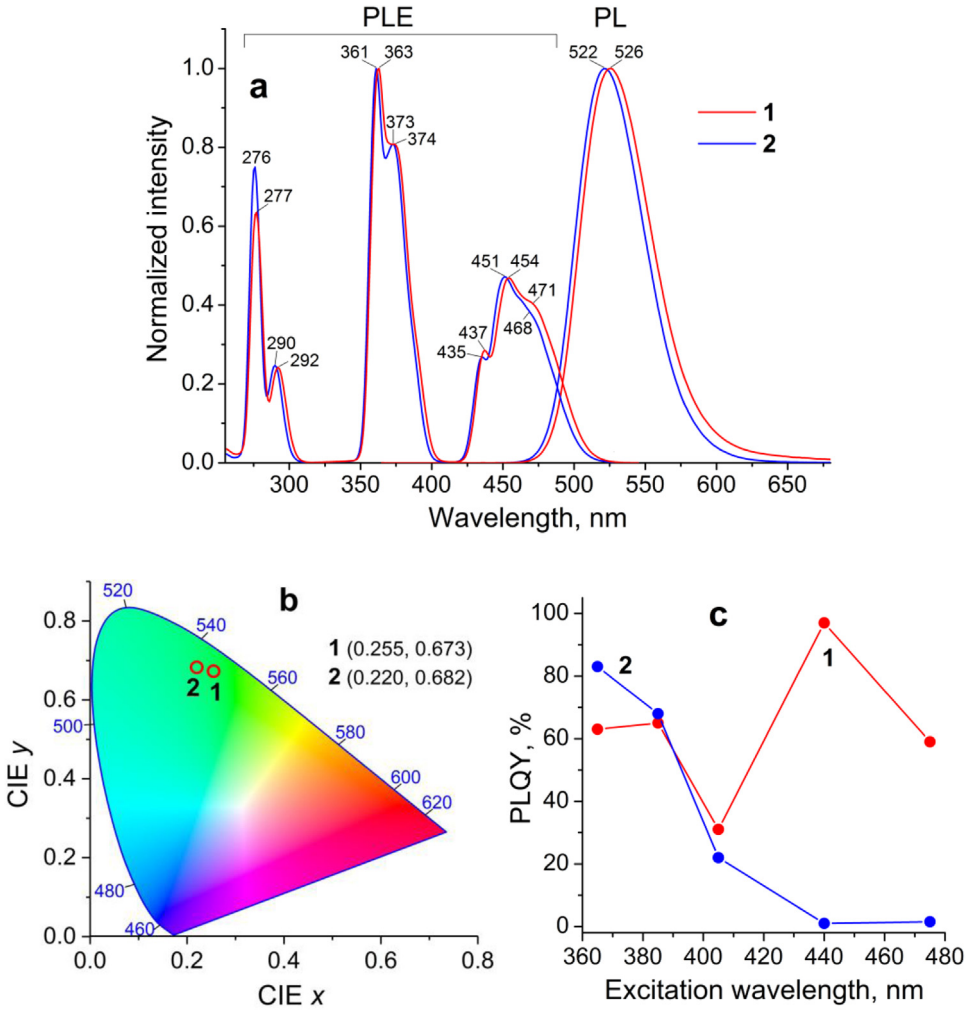

Fig. 3. PLE and PL spectra of **1** (blue) and **2** (red) at RT (a). CIE 1931 color space chromaticity diagram in the (*x*, *y*) coordinates (b). The dependence of PLQY on different excitation wavelengths (c).

S6), which joint $C_5H_{13}N_2S^+$ ions with $MnBr_4^{2-}$ polyhedra and form 3D net.

The $(C_7H_{17}N_2S)_2[MnBr_4]$ compound crystallizes in the monoclinic space group of *C*2/*c*. As shown in Fig. 2a, the crystallographic asymmetric unit of **2** consists of one $C_7H_{17}N_2S^+$ ion, a half of Mn^{2+} and two Br^- ions. As in **1**, the Mn^{2+} ion in **2** is surrounded by four bromide ions and forms isolated $MnBr_4^{2-}$ tetrahedron. (Fig. 2). The Mn–Br bond lengths (2.5064(13) and 2.5231(13) Å) and the Br–Mn–Br bond angles (from 107.11(3) to 114.61(8)°) are close to those found in the reported $MnBr_4^{2-}$ tetrahedrons [4–27]. The closest Mn···Mn distance within the crystal is 8.7324(12) Å. There are two N–H···Br and two S–H···Br hydrogen bonds (Fig. 2, Table S7) joint the $C_7H_{17}N_2S^+$ ions with tetrahedral $MnBr_4^{2-}$ ions and form 3D net. As in **1** (Fig. 1a), hydrogen bonds in **2** form identical six-membered rings (Fig. 2b) corresponding to the supramolecular motif R_2^1 [38]. In summary, in **1** and **2** there are similar hydrogen bonds between the counterions. We calculated the distortion parameters of $MnBr_4$ tetrahedra [7] in these compounds. The bond length distortion (Δd) is calculated to be 2.62×10^{-5} in **1** and 1.10×10^{-5} in **2**. The bond angle distortion (σ_{tet}^2) is calculated to be 3.58 in **1** and 7.70 in **2**.

3.2. Stability of compounds 1 and 2

To determine the overall stability of the synthesized compounds, their thermal decomposition under the dynamic argon atmosphere was studied. The $(C_5H_{13}N_2S)_2[MnBr_4]$ begins to melt at 81.5°C (Fig. S3), and upon cooling of the melt, it reversibly transforms into the starting luminescent compound. The endothermic effect at 92.3°C corresponds to this process. Decomposition of the compound with loss of mass occurs at temperatures above 130°C. The $(C_7H_{17}N_2S)_2[MnBr_4]$ has a melting point of 120°C (Fig. S4); on the DSC curve, an endothermic effect at 135.3°C corresponds of this phase transition. The substance starts to decompose at temperature above 150°C. The composition of the decomposition products was not established.

The stability of the materials in air varies. In air, the powder of **1** hygroscopic and irreversibly absorbs water, turning into a liquid state within a few days. However, large crystals in a closed vessel are stable for at least 6 months. In contrast to **1**, the compound **2** is stable in air at least 6 months, which can be explained by the more hydrophobic nature of its organic component.

3.3. Photoluminescent properties

While illuminated by a UV lamp, the compounds **1** and **2** emit bright green light, as presented in Fig. S5. To reveal the photoluminescent properties, the absorption (Fig. S6), PLE (Figs. 3a, S8) and PL spectra (Fig. 3a) of $(C_5H_{13}N_2S)_2[MnBr_4]$ and $(C_7H_{17}N_2S)_2[MnBr_4]$ are investigated at room temperature. The energy band gap for the synthesized crystals was estimated to be 2.44 and 2.39 eV for **1** and **2**, respectively, from the absorption

spectrum in terms of the Tauc plot (Figs. S6a and S6b). The band gap for the organic ligand is much higher (4.53-4.63 eV) with a corresponding absorption peak around 220-245 nm (Fig. S6), which belongs to the $\pi-\pi^*$ transition of the thioureas ligand. PLE spectrum of **1** is slightly red shifted (1-3 nm) compared to **2**. At the same time, the excitation spectrum does not depend on the emission wavelength in the range of 500–550 nm (Fig. S7a). Three distinct groups of excitation bands that belong to different spectral ranges (265-310, 345-405, 420-520 nm) with the peaks at 276-277 nm, 290-292 nm, 361-363 nm, 373-374 nm, 435-437 nm, 451-454 nm and shoulder near 468-471 nm can be distinguished in Fig. 3a. These PLE peaks can be attributed (Fig. S8) to the electronic transitions of Mn^{2+} from the ground state of $^6A_1$ to the various excited states of ^4F, ^4P, ^4D and ^4G in the tetrahedral $[MnBr_4]^{2-}$ [39]. The bands of ^4G states (420-520 nm) are not resolved as clearly as in the other two groups, and the intensity of this group is lower. The peaks in the absorption spectrum in the range of 285-480 nm are close to the bands observed in the PLE spectrum (Fig. S9) and can be attributed to the same Mn^{2+} transitions [40].

The powders **1** and **2** show green luminescence in the range of 470-650 nm (Fig. 3a). The calculated CIE coordinates for $(C_5H_{13}N_2S)_2[MnBr_4]$ and $(C_7H_{17}N_2S)_2[MnBr_4]$ emission are (0.255, 0.673) and (0.220, 0.682), respectively (Fig. 3b). The PL spectra of **1** and **2** with peaks at 526 nm and 522 are rather narrow (FWHM 55–57 nm). Stokes shift is calculated from the PLE and PL peaks and is 71-72 nm (0.38 eV) for both powders. The PL maximum of emission of these compounds corresponds to the wavelength range characteristic of other Mn^{II}-based tetrahedral HMHs [3,9,12,13]. Of the N- and N,N'-substituted thioureas, only the aromatic ligands are characterized by very weak emissions around 450 nm and a significant contribution of the N,N'-dialkylsubstituted thioureas to the emission in **1**-**2** is excluded [41,42]. The PL spectrum of **1** is slightly red shifted (4 nm) in comparison with **2**, as in the PLE spectrum. The emission peak does not shift depending on different excitation wavelengths in the range of 275-435 nm (Fig. S7b), confirming the intrinsic emission properties of the $(C_5H_{13}N_2S)_2[MnBr_4]$ and $(C_7H_{17}N_2S)_2[MnBr_4]$ crystals originating from Mn^{2+} emission centers. The coincidence of the PLE and PL spectra for **1–2** also agrees with the conclusion that PL arises due to the Mn^{2+} ions. The photoluminescence band at 522-526 nm for **1** and **2** can be attributed to the forbidden $^4T_1(G) \rightarrow {}^6A_1$ transition of the tetrahedrally coordinated Mn^{2+} ion [2–13]. Synthesized hybrid manganese bromides produce a weak electron-phonon coupling and crystal field strength, which leads to narrow-band emission of 55–57 nm FWHM with a small Stokes shift of 71-72 nm [39]. The similarity of the PL and PLE spectra for **1** and **2** can be explained by the coincidence of the hydrogen bonds system that form the same nearest atomic environment of the emitting $MnBr_4^{2-}$ centers.

The PLQY for **1-2** is not monotonically dependent on the excitation wavelength. The powder of $(C_5H_{13}N_2S)_2[MnBr_4]$ showed PLQY equal to 63%, 65%, 31%, 97%, and 59% under 365, 385, 405, 440 and 475 nm excitation, respectively (Fig. 3c). The PLQY of $(C_5H_{13}N_2S)_2[MnBr_4]$ is highest when excited within the lowest energy PLE band (around 440 nm). The Mn···Mn distance is a highly dominant factor for the PLQY in this class of materials [3,22]. High PLQY (97%) for **1** indicates that concentration quenching of the luminescence in the system of Mn(II) ions is practically absent at the characteristic distance of 8.11 Å (Fig. 1b). A high average Mn···Mn distance is advantageous for a higher PLQY due to the reduction of energy transfer processes between neighboring Mn centers, which reduces the concentration quenching of the luminescence. The powder of $(C_7H_{17}N_2S)_2[MnBr_4]$ showed PLQY equal to 83%, 68% and 22% under 365, 385 and 405 nm excitation (Fig. 3c), respectively. Although the shortest distance Mn···Mn (8.73 Å) for **2** is greater than for **1** (8.11 Å), however, the quantum yield for **2** turned out to be much lower at higher excitation wavelengths. The observed discrepancy can be explained by the different influence of other factors on PLQY, for example, the organic cation nature, the crystals symmetry, and degree of distortion in MnX_4^{2-}.

4. Conclusions

In summary, protonated N,N'-dialkylthioureas were successfully introduced into the composition of organic-inorganic metal halides as new representatives of the organic cations. Two novel lead-free hybrid organic–inorganic metal halides $(C_5H_{13}N_2S)_2[MnBr_4]$ (**1**) and $(C_7H_{17}N_2S)_2[MnBr_4]$ (**2**) were synthesized and characterized. The 0D crystal structures of these compounds consist of discrete tetrahedral $[MnBr_4]^{2-}$ anions, organic cations $C_5H_{13}N_2S^+$ (in **1**) and $C_7H_{17}N_2S^+$ (in **2**). The counterions are connected by electrostatic attraction and intermolecular N–H···Br and S–H···Br hydrogen bonds. The hydrogen bonds system of these compounds is the same, which explains the similarity of PL and PLE spectra. The observed excitation-independent PL spectra are indicative of a single mechanism of radiative transition. A green emission peaking at 526 nm for **1** and 522 nm for **2** with a high PLQY at room temperature is attributed to the $^4T_1(G)$ to $^6A_1$ radiative transition of tetrahedrally coordinated Mn^{2+} ions in the $[MnBr_4]^{2-}$ unit. Our results show that N,N'-dialkylthioureas are promising components in hybrid organic-inorganic halides and provide a design principle for the discovery of highly efficient, light-emitting materials.

Declaration of Competing Interest

The authors declare the following financial interests/personal relationships which may be considered as potential competing interests Maxim Molokeev reports financial support was provided by Russian Foundation for Basic Research.

CRediT authorship contribution statement

Nicolay N. Golovnev: Supervision, Writing – original draft, Writing – review & editing, Conceptualization. **Marina A. Gerasimova:** Data curation, Formal analysis, Writing – review & editing. **Ivan A. Ostapenko:** Data curation, Formal analysis. **Andrey O. Zolotov:** Data curation, Formal analysis. **Maxim S. Molokeev:** Supervision, Writing – original draft, Writing – review & editing, Conceptualization, Funding acquisition, Data curation, Formal analysis.

Data availability

Data will be made available on request.

Acknowledgements

The reported study was funded by RFBR according to the research project № 19-52-80003. X-ray data from single crystals and powders were obtained with the analytical equipment of Krasnoyarsk Center of collective use of SB RAS.

Supplementary materials

Supplementary material associated with this article can be found, in the online version, at doi:10.1016/j.molstruc.2022.134851.

References

[1] K. Nikolič, F. Lignou, H.P. de la Garanderie, Luminescence spectra in tetrahalomanganate complexes, J. Lumin. 8 (1973) 137–148, doi:10.1016/0022-2313(73)90100-2.
[2] Y. Qin, P. She, X. Huang, W. Huang, Q. Zhao, Luminescent manganese(II) complexes: Synthesis, properties and optoelectronic applications, Coord. Chem. Rev. 416 (2020) 213331, doi:10.1016/j.ccr.2020.213331.

[3] B. Su, G. Zhou, J. Huang, E. Song, A. Nag, Z. Xia, Mn^{2+}-doped metal halide perovskites: structure, photoluminescence, and application, Laser Photonics Rev 15 (2021) 2000334, doi:10.1002/lpor.202000334.

[4] C. Jiang, N. Zhong, C. Luo, H. Lin, Y. Zhang, H. Peng, C.-G. Duan, Diisopropylammonium)$_2$$MnBr_4$: a multifunctional ferroelectric with efficient green-emission and excellent gas sensing properties, Chem. Commun. 53 (2017) 5954–5957, doi:10.1039/C7CC01107E.

[5] P. Fu, Y. Sun, Z. Xia, Z. Xiao, Photoluminescence behavior of zero-dimensional manganese halide tetrahedra embedded in conjugated organic matrices, J. Phys. Chem. Lett. 12 (2021) 7394–7399, doi:10.1021/acs.jpclett.1c02154.

[6] A.S. Berezin, M.P. Davydova, D.G. Samsonenko, T.S. Sukhikh, A.V. Artem'ev, A family of brightly emissive homo- and mixed-halomanganates(II): The effect of halide on optical and magnetic properties, J. Lumin. 236 (2021) 118069, doi:10.1016/j.jlumin.2021.118069.

[7] D.P. Panda, D. Swain, A. Sundaresan, Zero-dimensional (piperidinium)$_2$$MnBr_4$: Ring puckering-induced isostructural transition and strong electron−phonon coupling mediated self-trapped exciton emission, Inorg. Chem. 61 (2022) 11377–11386, doi:10.1021/acs.inorgchem.2c01601.

[8] H. Zhang, Y.-H. Tan, Y.-Z. Tang, X.-W. Fan, X.-L. Peng, R.-R. Han, Y.-K. Li, F.-X. Wang, Two manganese(II)-based hybrid multifunctional phase transition materials with strong photoluminescence, high quantum yield, and switchable dielectric properties: $(C_6NH_{16})_2MnBr_4$ and $(C_7NH_{18})_2MnBr_4$, Inorg. Chem. 61 (2022) 10454–10460, doi:10.1021/acs.inorgchem.2c01276.

[9] S. Chen, J. Gao, J. Chang, Y. Zhang, L. Feng, Organic-inorganic manganese (II) halide hybrids based paper sensor for the fluorometric determination of pesticide ferbam, Sensor. Actuat. B-Chem. 297 (2019) 126701, doi:10.1016/j.snb.2019. 126701.

[10] H. Yu, Y.X. Mei, Z.H. Wei, G.Q. Mei, H. Cai, Fluorescent properties of manganese halide benzothiazole inorganic-organic hybrids, J. Fluoresc. 26 (2016) 2295–2301, doi:10.1007/s10895-016-1925-x.

[11] Y.-L. Wei, J. Jing, C. Shi, H.-Y. Ye, Z.-X. Wang, Y. Zhang, High quantum yield and unusual photoluminescence behaviour in tetrahedral manganese(II) based on hybrid compounds, Inorg. Chem. Front. 5 (2018) 2615–2619, doi:10.1039/C8QI00793D.

[12] A. Jana, S. Zhumagali, Q. Ba, A.S. Nissimagoudar, K.S. Kim, Direct emission from quartet excited states triggered by upconversion phenomena in solid-phase synthesized fluorescent lead-free organic-inorganic hybrid compounds, J. Mater. Chem. A 7 (2019) 26504–26512, doi:10.1039/C9TA08268A.

[13] V. Morad, I. Cherniukh, L. Pöttschacher, Y. Shynkarenko, S. Yakunin, M.V. Kovalenko, Manganese(II) in tetrahedral halide environment: factors governing bright green luminescence, Chem. Mater. 31 (2019) 10161–10169, doi:10.1021/acs.chemmater.9b03782.

[14] J. Chen, Q. Zhang, F.K. Zheng, Z.F. Liu, S.-H. Wang, A.-Q. Wu, G.-C. Guo, Intense photo- and tribo-luminescence of three tetrahedral manganese(II) dihalides with chelating bidentate phosphine oxide ligand, Dalton Trans. 44 (2015) 3289–3294, doi:10.1039/C4DT03694H.

[15] C. Jiang, H. Fu, Y. Han, D. Li, H. Lin, B. Li, X. Meng, H. Peng, J. Chu, Tuning the crystal structure and luminescence of pyrrolidinium manganese halides via halide ions, Cryst. Res. Tech. 54 (2019) 1800236, doi:10.1002/crat.201800236.

[16] A.S. Berezin, D.G. Samsonenko, V.K. Brel, A.V. Artem'ev, Two-in-one" organic–inorganic hybrid Mn^{II} complexes exhibiting dual-emissive phosphorescence, Dalton Trans 47 (2018) 7306–7315, doi:10.1039/C8DT01041B.

[17] Y. Rodríguez-Lazcano, L. Nataf, F. Rodríguez, Electronic structure and luminescence of $[(CH_3)_4N]_2MnX_4$ (X = Cl, Br) crystals at high pressures by time-resolved spectroscopy: pressure effects on the Mn-Mn exchange coupling, Phys. Rev. B Condens. Matter 80 (2009) 085115, doi:10.1103/PhysRevB.80.085115.

[18] S. Pitula, A.-V. Mudring, Synthesis, structure, and physico-optical properties of manganate(II)-based ionic liquids, Chem. Eur. J. 16 (2010) 3355–3365, doi:10.1002/chem.200802660.

[19] P. Singh, P.J.S. Rana, P. Dhingra, P. Kar, Towards toxicity removal in lead based perovskite solar cells by compositional gradient using manganese chloride, J. Mater. Chem. C 4 (2016) 3101–3105, doi:10.1039/C6TC00650G.

[20] L.-J. Xu, C.-Z. Sun, H. Xiao, Y. Wu, Z.-N. Chen, Green-light-emitting diodes based on tetrabromide manganese(II) complex through solution process, Adv. Mater. 29 (2017) 1605739, doi:10.1002/adma.201605739.

[21] S. Wang, X. Han, T. Kou, Y. Zhou, Y. Liang, Z. Wu, J. Huang, T. Chang, C. Peng, Q. Wei, B. Zou, Lead-free Mn^{II}-based red-emitting hybrid halide $(CH_6N_3)_2MnCl_4$ toward high performance warm WLEDs, J. Mater. Chem. C 9 (2021) 4895–4902, doi:10.1039/D1TC00632K.

[22] L. Mao, P. Guo, S. Wang, A.K. Cheetham, R. Seshadri, Design principles for enhancing photoluminescence quantum yield in hybrid manganese bromides, J. Am. Chem. Soc. 142 (2020) 13582–13589, doi:10.1021/jacs.0c06039.

[23] Y. Guo, J. Wu, W. Liu, S.-P. Guo, Organic cation modulation triggered second harmonic response in manganese halides with bright fluorescence, Inorg. Chem. 61 (2022) 11514–11518, doi:10.1021/acs.inorgchem.2c01796.

[24] M.D. Smith, B.A. Connor, H.I. Karunadasa, Tuning the luminescence of layered halide perovskites, Chem. Rev. 119 (2019) 3104–3139, doi:10.1021/acs.chemrev.8b00477.

[25] G. Zhou, Z. Liu, M.S. Molokeev, Z. Xiao, Z. Xia, X.-M. Zhang, Manipulation of Cl/Br transmutation in zero-dimensional Mn^{2+}-based metal halides toward tunable photoluminescence and thermal quenching behaviors, J. Mater. Chem. C 9 (2021) 2047–2053, doi:10.1039/D0TC05137C.

[26] P. Fu, Y. Sun, Z. Xia, Z. Xiao, Photoluminescence behavior of zero-dimensional manganese halide tetrahedra embedded in conjugated organic Matrices, J. Phys. Chem. Lett. 12 (2021) 7394–7399, doi:10.1021/acs.jpclett.1c02154.

[27] B. Li, Y. Xu, X. Zhang, K. Han, J. Jin, Z. Xia, Zero-dimensional luminescent metal halide hybrids enabling bulk transparent medium as large-area X-ray scintillators, Adv. Optical Mater. 10 (2022) 2102793, doi:10.1002/adom.202102793.

[28] W.C. Schiessla, N.K. Summa, C.F. Weber, S. Gubo, C. Dücker-Benfer, R. Puchta, N.J.R.E. Hommes, R. Eldik, Experimental and theoretical approaches to the protonation of thiourea: a convenient nucleophile in coordination chemistry revisited, Z. Anorg. Allg. Chem. 631 (2005) 2812–2819, doi:10.1002/zaac.200500157.

[29] M. Daub, H. Hillebrecht, First representatives of (210)-oriented perovskite variants − Synthesis, crystal structures and properties of the new 2D hybrid perovskites $A[HC(NH_2)_2]PbI_4$; A = $[C(NH_2)_3]$, $[HSC(NH_2)_2]$, Z. Kristallogr. Cryst. Mater. 233 (2018) 555–564, doi:10.1515/zkri-2018-2055.

[30] S.-K. Yu, N.-N. Xu, M. Jiang, Y.-G. Weng, Q.-Y. Zhu, J. Dai, Hybrid lead iodide perovskites with mixed cations of thiourea and methylamine, from one dimension to three dimensions, Inorg. Chem. 59 (2020) 15842–15847, doi:10.1021/acs.inorgchem.0c02280.

[31] M. Daub, H. Hillebrecht, From 1D to 3D: perovskites within the system $HSC(NH_2)_2I/CH_3NH_3I/PBI_2$ with maintenance of the cubic closest packing, Inorg. Chem. 60 (2021) 3082–3093, doi:10.1021/acs.inorgchem.0c03386.

[32] O.V. Rudnitskaya, E.K. Kultyshkina, E.V. Dobrokhotova, V.S. Podvoyskaya, P.V. Dorovatovskii, V.A. Lazarenko, Y.V. Zubavichus, V.N. Khrustalev, The synthesis, characterization, and structure of $(ThioH)_2[OsX_6]$ (X = Cl, Br), Polyhedron 134 (2017) 114–119, doi:10.1016/j.poly.2017.05.057.

[33] Ming Li, R.K. Li, Two new bismuth thiourea bromides: crystal structure, growth, and characterization, Dalton Trans. 43 (2014) 2577–2580, doi:10.1039/C3DT52953C.

[34] G.M. Sheldrick, A short history of SHELX, Acta Cryst. A. 64 (2008) 112–122, doi:10.1107/S0108767307043930.

[35] PLATON – A Multipurpose Crystallographic Tool, Utrecht University, Utrecht, The Netherlands, 2008.

[36] K. Brandenburg, M. Berndt, DIAMOND - Visual Crystal Structure Information System CRYSTAL IMPACT, Postfach 1251, D-53002 Bonn.

[37] Bruker AXS TOPAS V4: General profile and structure analysis software for powder diffraction data. – User's Manual, Bruker AXS, Karlsruhe, Germany, 2008.

[38] J.W. Steed, J.L. Atwood, Supramolecular Chemistry, Chichester: J. Wiley, UK, 2000.

[39] Q. Ren, J. Zhang, Y. Mao, M.S. Molokeev, G. Zhou, X.-M. Zhang, Ligand engineering triggered efficiency tunable emission in zero-dimensional manganese hybrids for white light-emitting diodes, Nanomaterials 12 (2022) 3142, doi:10.3390/nano12183142.

[40] S. Chen, J.Chang J..Gao, Y. Zhang, L. Feng, Organic-inorganic manganese (II) halide hybrids based paper sensor for the fluorometric determination of pesticide ferbam, Sens. Actuators B: Chem. 297 (2019) 126701, doi:10.1016/j.snb.2019.126701.

[41] F. Grifasi, M.R. Chierotti, C. Garino, R. Gobetto, E. Priola, E. Diana, F. Turci, Solvent-free synthesis of luminescent copper(I) coordination polymers with thiourea derivatives, Cryst. Growth Des. 15 (2015) 2929–2939, doi:10.1021/acs.cgd.5b00352.

[42] N.N. Golovnev, A.S. Aleksandrovsky, M.A. Gerasimova, F.N. Tomilin, V.A. Mironov, A.V. Demina, Z. Xia, M.S. Molokeev, Luminescent zero-dimensional hybrid lead thiohalide nanostructures for high quantum yield and broadband excitation, ACS Appl. Nano Mater. 4 (2021) 3654–3663, doi:10.1021/acsanm.1c00162.